

# Phase diagram of truncated tetrahedral model

Roman KRCMAR<sup>1</sup>, Andrej GENDIAR<sup>1,\*</sup> and Tomotoshi NISHINO<sup>2</sup>

<sup>1</sup>*Institute of Physics, Slovak Academy of Sciences, SK-845 11, Bratislava, Slovakia and*

<sup>2</sup>*Department of Physics, Graduate School of Science, Kobe University, Kobe 657-8501, Japan*

(Dated: February 27, 2019)

Phase diagram of a discrete counterpart of the classical Heisenberg model, the truncated tetrahedral model, is analyzed on the square lattice, when the interaction is ferromagnetic. Each spin is represented by a unit vector that can point one of the 12 vertices of the truncated tetrahedron, which is a continuous interpolation between the tetrahedron and the octahedron. Phase transition of the model is determined by means of entanglement entropy, which is numerically calculated by the corner transfer matrix renormalization group method. The obtained phase diagram consists of four different phases, which are separated by five transition lines. The feature of each phase transition line is investigated.

PACS numbers: 75.10.Pq, 75.40.Mg

## I. INTRODUCTION

Symmetry breaking is one of the fundamental concepts in the field theoretical analyses. Phase transitions in statistical models are known as typical realizations of the symmetry breaking, where the feature of transitions is dependent on symmetries in local degrees of freedom. For example, the classical Heisenberg model has the  $O(3)$  symmetry, and the continuous symmetry prohibits phase transition at finite temperature when the model is on two-dimensional (2D) lattices<sup>1</sup>. The  $O(3)$  symmetry group has discrete subgroups, some of which correspond to polyhedral symmetries, including tetrahedral and octahedral ones as examples. Discrete counterpart of the classical Heisenberg model can be defined according to these discrete group symmetries, where the corresponding spin systems are known as the polyhedral models. It should be noted that such discrete models can undergo phase transitions at finite temperature, if the neighboring interaction is ferromagnetic. For example, the ferromagnetic tetrahedral model on the square lattice exhibits the phase transition subject to the 4-state Potts universality class<sup>2</sup>.

A theoretical interest on the polyhedral models is in the case where the discrete symmetry group has subgroups. In such a case successive transitions from a phase with higher symmetry to another phase with lower symmetry can be observed; the symmetry is only partially broken in the intermediate temperature region<sup>3,4</sup>. Surungan *et al.* investigated a discrete counterpart of the Heisenberg model, the edge-cubic model, in which the local spins can point one of the 12 vertices of the cuboctahedron<sup>4</sup>. They detected two phase transitions; in the low-temperature side, there is a phase transition subject to the 3-state Potts universality class, and in the high-temperature side, there is another phase transition, which could be explained by the cubic symmetry. The edge-cubic model belongs to a variety of truncated platonic solid models, which can also be regarded as discrete counterparts to the classical Heisenberg model. In this work we investigate another example of the truncated

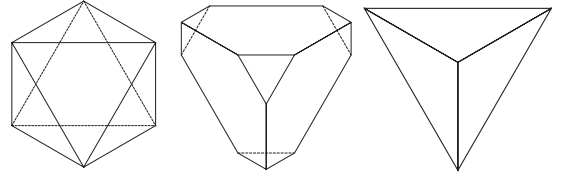


FIG. 1. The truncated tetrahedron (middle,  $t = 0.5$ ), as a continuous interpolation between octahedron (left,  $t = 0$ ) and the tetrahedron (right,  $t = 1$ ).

models, the truncated tetrahedral model (TTM), which is a continuous interpolation between the tetrahedral and the octahedral models.

This article is organized as follows. In the next section we introduce the TTM, and briefly discuss its property around the octahedral and the tetrahedral limits. In Section III, the phase diagram in the entire parameter region is determined by means of the entanglement entropy, which is calculated by the Corner Transfer Matrix Renormalization Group (CTMRG) method<sup>5,6</sup>. We then classify the nature of the phase transition lines. The obtained results are summarized in the last section.

## II. TRUNCATED TETRAHEDRAL MODEL

We consider a finite-directional counterpart of the classical Heisenberg model on the 2D square lattice. Local spin on each lattice site is represented by a unit vector that can point one of the 12 vertices of the truncated tetrahedron shown in Fig. 1, whose shape is determined by a parameter  $t$  from octahedral limit  $t = 0$  to the tetrahedral one  $t = 1$ . We represent the spin variable on the site that is specified by indices  $i$  and  $j$  by means of the unit vector  $\mathbf{S}_{i,j}(t)$  given by

$$\mathbf{S}_{i,j}(t) = \sqrt{\frac{1+2t^2}{2}} \mathbf{s}^{[k]}(t), \quad (1)$$

TABLE I. The directions of the 12 vertices of the truncated tetrahedron represented by means of the unnormalized vector  $\mathbf{s}^{[k]}(t)$ .

$k$	$\mathbf{s}^{[k]}(t)$	$k$	$\mathbf{s}^{[k]}(t)$
1	$\left( t, 0, -\frac{1}{\sqrt{2}} \right)$	2	$\left( -t, 0, -\frac{1}{\sqrt{2}} \right)$
3	$\left( \frac{1-t}{2}, \frac{1+t}{2}, \frac{t}{\sqrt{2}} \right)$	4	$\left( \frac{1+t}{2}, \frac{1-t}{2}, -\frac{t}{\sqrt{2}} \right)$
5	$\left( -\frac{1+t}{2}, \frac{1-t}{2}, -\frac{t}{\sqrt{2}} \right)$	6	$\left( -\frac{1-t}{2}, \frac{1+t}{2}, \frac{t}{\sqrt{2}} \right)$
7	$\left( -\frac{1-t}{2}, -\frac{1+t}{2}, \frac{t}{\sqrt{2}} \right)$	8	$\left( -\frac{1+t}{2}, -\frac{1-t}{2}, -\frac{t}{\sqrt{2}} \right)$
9	$\left( \frac{1-t}{2}, -\frac{1+t}{2}, \frac{t}{\sqrt{2}} \right)$	10	$\left( \frac{1+t}{2}, -\frac{1-t}{2}, -\frac{t}{\sqrt{2}} \right)$
11	$\left( 0, t, \frac{1}{\sqrt{2}} \right)$	12	$\left( 0, -t, \frac{1}{\sqrt{2}} \right)$

where the components of unnormalized vector  $\mathbf{s}^{[k]}(t)$  for  $k = 1 \sim 12$  are listed in Table I. We assume that ferromagnetic coupling  $J > 0$  is present between nearest-neighbor sites, and that the interaction is represented in the form of inner product. Under these settings, the Hamiltonian of the TTM is written as

$$H_t = -J \sum_{i,j} \left[ \mathbf{s}_{i,j}(t) \cdot \mathbf{s}_{i+1,j}(t) + \mathbf{s}_{i,j}(t) \cdot \mathbf{s}_{i,j+1}(t) \right]. \quad (2)$$

As it is shown in Fig. 1, the TTM reduces to the tetrahedral model in the limit  $t = 1$ , apart from the multiplicity of 3 for each tetrahedron vertices. One can check the equivalence  $\mathbf{s}^{[1]}(1) = \mathbf{s}^{[4]}(1) = \mathbf{s}^{[10]}(1)$  from Table I, and the same for the groups  $k = 2, 5, 8, k = 3, 6, 11$ , and  $k = 7, 9, 12$ . The tetrahedral model is essentially equivalent to the 4-state Potts model. In another limit  $t = 0$ , the TTM reduces to the octahedral model; in this case  $k = 1, 2, k = 3, 4, k = 5, 6, k = 7, 8, k = 9, 10$ , and  $k = 11, 12$  are the 6 direction of the octahedron vertices.

In order to obtain the phase diagram with respect to the parameter  $t$  and the temperature  $T$ , we calculate the free energy of the TTM. Let us consider the finite size system of the size  $L$  by  $L$ . The partition function

$$Z_t(T; L) = \sum_{\{\mathbf{S}(t)\}} \exp \left( -\frac{H_t}{k_B T} \right) \quad (3)$$

is the configuration sum of Boltzmann factor taken over all the spins denoted by  $\{\mathbf{S}(t)\}$ . Here,  $k_B$  is Boltzmann constant, and we use the dimensionless units by setting  $k_B = J = 1$ . Once  $Z_t(T; L)$  is obtained for a series of system size  $L$ , we can estimate the free energy per site

$$f_t(T) = \lim_{L \rightarrow \infty} -\frac{1}{L^2} k_B T \ln Z_t(T; L) \quad (4)$$

in the thermodynamic limit.

As a numerical tool to obtain  $Z_t(T; L)$ , we use the CTMRG method, which was developed from Baxter's

corner transfer matrix (CTM) formalism<sup>7</sup>. The method enables to calculate the partition function in the form

$$Z_t(T; L) = \text{Tr } C^4, \quad (5)$$

where  $C$  is the CTM, which corresponds to a quadrant of the finite system<sup>5,6</sup>. It is convenient to define the normalized density matrix

$$\rho(T; L) = \frac{C^4}{\text{Tr } C^4} = \frac{C^4}{Z_t}, \quad (6)$$

and the mean value of a local operator  $O$  at the center of the system is given by  $\langle O \rangle = \text{Tr}(O\rho)$ . In the CTMRG calculations, we keep  $m = 300$  representative states at most. Further details of the free energy analysis by CTMRG can be found in Ref. 8.

The 2D classical systems can be related to one-dimensional quantum systems via the Suzuki-Trotter decomposition<sup>9-11</sup>. This quantum-classical correspondence<sup>12</sup> enables us to introduce the notions of quantum information, such as the concurrence<sup>13,14</sup> and the entanglement entropy<sup>14-16</sup> to 2D classical systems. The entanglement entropy in the current study is represented as

$$S_v(T; L) = -\text{Tr } \rho \ln \rho \sim -\sum_{k=1}^m \lambda_k \ln \lambda_k, \quad (7)$$

where  $\lambda_k$  are the eigenvalues of the density matrix  $\rho(T; L)$  in Eq. (6). It is known that close to a critical point, the entanglement entropy scales as  $S_v(T; \infty) \sim \frac{c}{6} \ln \xi$ , where  $c$  is a central charge and  $\xi$  is the correlation length<sup>17,18</sup>. Thus  $S_v(T; \infty)$  is divergent at the critical point, and can be used for finding the location of phase boundaries. In the case of first-order phase transition,  $S_v(T; \infty)$  is discontinuous at the transition point. As examples, we show  $S_v(T; L)$  when  $L = 1000$  for the cases  $t = 0.2, 0.3$ , and  $0.4$  with respect to temperature  $T$  in Fig. 2. It should be noted that there is no need to observe thermodynamic functions for the determination of the phase boundary.

### III. PHASE DIAGRAM

Figure 3 shows the phase diagram of the TTM determined from the singular or discontinuous behavior in  $S_v$  as shown in Fig. 2. There are 4 phases, which are labeled from I to IV in the diagram. In the low-temperature side, there is a ferromagnetic phase I, where the symmetry is totally broken. The intermediate phase II in the octahedral side has the  $Z_2$  symmetry, and if the directions  $k = 1$  and  $k = 2$  according to Table I are spontaneously chosen, these two directions appear equally. The intermediate phase III in the tetrahedral side has the  $D_3$  symmetry, and if the directions  $k = 1, k = 4$ , and  $k = 10$  are spontaneously chosen, these three directions appear equally. The phase IV in the high temperature side is completely disordered. The phase boundaries shown by

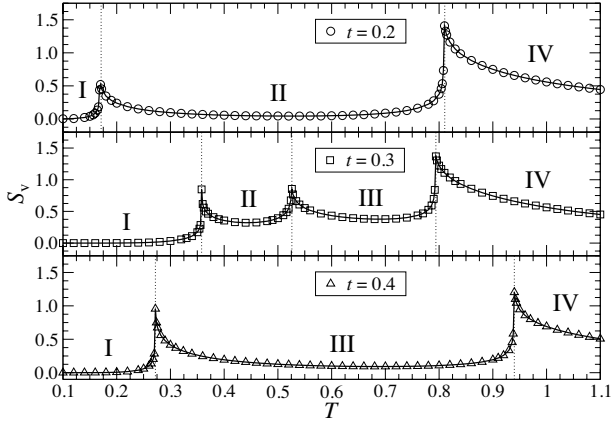


FIG. 2. The temperature dependence of the entanglement entropy  $S_v$  for  $t = 0.2$ ,  $t = 0.3$ , and  $t = 0.4$ . The vertical dotted lines denote phase boundaries, and each phase is labeled by the roman number.

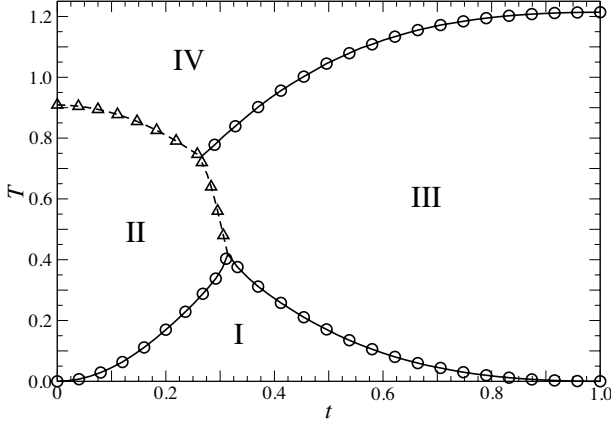


FIG. 3. Phase diagram of the TTM with respect to the parameter  $t$  and the temperature  $T$ . The circles denote the 2<sup>nd</sup> order phase transition. The phase boundaries shown by triangles are identified as the 1<sup>st</sup> order ones.

the circles are of the second-order phase transition, and those shown by the triangles are identified as first-order ones. We observe the detail of each phase boundary in the following.

Let us observe the phase boundary between the phases I and II, and also the boundary between the phases I and III. When the transition is of the second order, its universality can be determined by means of finite-size corrections in thermodynamic functions<sup>19,20</sup>. We consider the internal energy per site

$$u_t(T; L) = \frac{T^2}{L^2} \frac{\partial}{\partial T} \{k_B \ln Z_t(T; L)\} \quad (8)$$

as an example. At the critical temperature  $T_c$ , the internal energy per site satisfies

$$u_t(T_c; L) - u_t(T_c; \infty) \equiv \Delta u_t(L) \propto L^{1/\nu-2}, \quad (9)$$

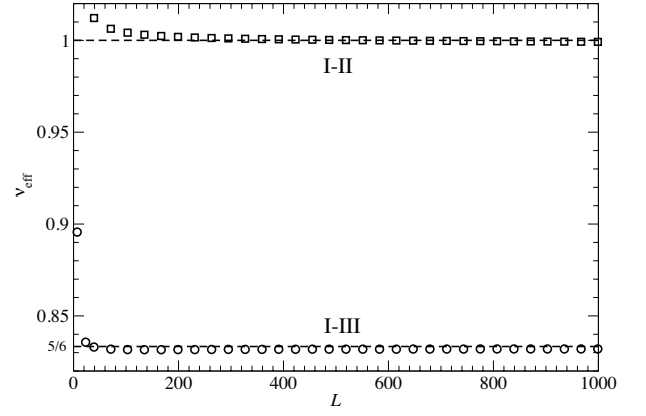


FIG. 4. The effective exponent  $\nu_{\text{eff}}(L)$  in Eq. (10) calculated at the I-II phase boundary when  $t = 0.1$  (squares), and that at the I-III boundary when  $t = 0.35$  (circles).

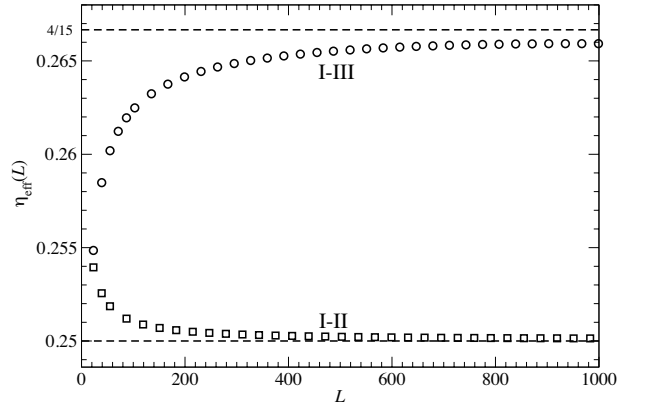


FIG. 5. The effective exponent  $\eta_{\text{eff}}(L)$  in Eq. (12) calculated at the I-II phase boundary when  $t = 0.1$  (squares), and that at the I-III boundary when  $t = 0.35$  (circles).

where  $\nu$  is the scaling exponent for the correlation length. One can obtain  $\nu$  observing the  $L$ -dependence of the effective value

$$\nu_{\text{eff}}(L) = \left[ 2 + \frac{\partial \ln \Delta u_t(L)}{\partial \ln L} \right]^{-1}, \quad (10)$$

which is shown in Fig. 4. The results agree with the Ising universality with  $\nu = 1$  for the I-II phase boundary ( $t = 0.1$ ), and the 3-state Potts universality with  $\nu = 5/6$  for the I-III boundary ( $t = 0.35$ ).

In order to obtain another scaling exponent, we observe an appropriate order parameter  $O_t(T; L)$ , for which the finite-size correction satisfies the relation

$$O_t(T_c; L) \equiv \Delta O_t(L) \propto L^{-\eta/2} \quad (11)$$

noticing that  $O_t(T_c; \infty)$  is zero. In the same manner as we have considered in Eq. (10), we can obtain  $\eta$  from the effective value

$$\eta_{\text{eff}}(L) = -2 \frac{\partial \ln \Delta O_t(L)}{\partial \ln L}. \quad (12)$$

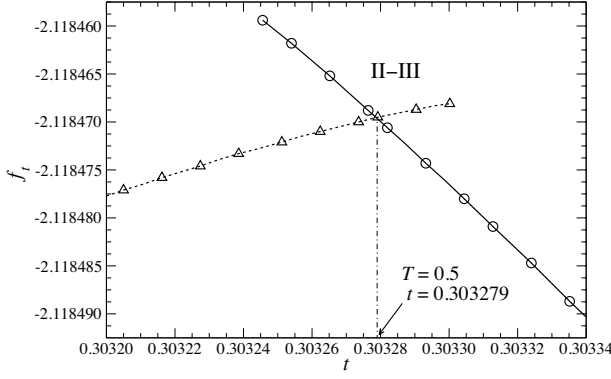


FIG. 6. The free energy per site  $f_t(T)$  with respect to the parameter  $t$  at fixed temperature  $T = 0.5$  under the fixed (triangles) and the free (circles) boundary conditions.

Inside the phase II we choose the order parameter

$$O_t(L) = p_1 + p_2 + p_3 + p_4 - 2p_5 - 2p_6 + p_7 + p_8 - 2p_9 - 2p_{10} + p_{11} + p_{12}. \quad (13)$$

where  $p_k$  are the probability of the spin at the center of the system to point  $k$ -th direction listed in Table I. Inside the phase III we choose

$$O_t(L) = p_1 - p_2 + p_3 - p_4 + p_5 - p_6 + p_7 - p_8 + p_9 - p_{10} + p_{11} - p_{12}. \quad (14)$$

Figure 5 shows the system size dependence of  $\eta_{\text{eff}}(L)$ . The behavior at the I-II phase boundary ( $t = 0.1$ ) agrees with Ising universality class with  $\eta = 1/4$ . At the I-III boundary, the convergence with respect to  $L$  is rather slow, but  $\eta_{\text{eff}}(L)$  certainly approaches to the value  $\eta = 4/15$  of the 3-state Potts universality class.

We next observe the II-III phase boundary in the intermediate temperature region. Figure 6 shows the crossover in the free energy per site  $f_t(T)$  at  $T = 0.5$  with respect to  $t$ , where the crossing point is  $t = 0.303279$ . We have chosen both fixed and free boundary conditions to weakly favor one of the two phases. Since the  $Z_2$  symmetry in the phase II and  $D_3$  symmetry in the phase III are not a sub-group with each another, a direct second-order phase transition between these phases is prohibited. It should be noted that the II-III boundary is not vertical in Fig. 3.

Figure 7 shows the calculated free energy per site  $f_{t=0}(T)$  at the octahedral limit  $t = 0$ , which are calculated under the fixed and the free boundary conditions. Within the shown temperature region, the lower plots are thermodynamically stable, and the upper ones are quasi-stable. These two lines crosses at  $T_0 = 0.908413$ . This crossover in  $f_{t=0}(T)$  shows that the transition is of the first-order. At the transition temperature  $T_0$ , the internal energy per site  $u_t(T; L)$  in Eq. (15) is discontinuous in the thermodynamic limit. From the jump in  $u_t(T; L)$  when  $L$  is sufficiently large, we obtain the latent heat  $Q = 0.073$ . Figure 8 shows  $f_{t=0.2}(T)$  when  $t = 0.2$ .

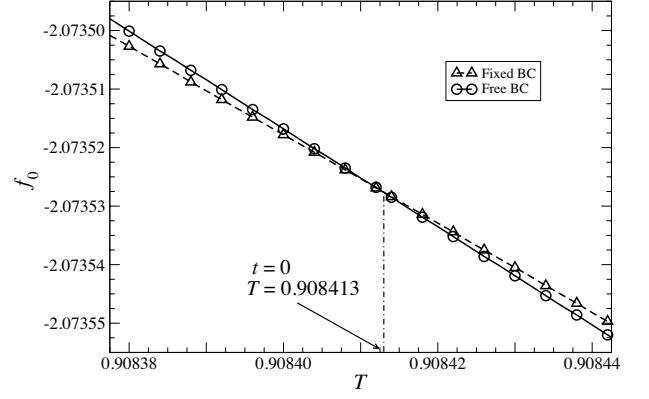


FIG. 7. Temperature dependence of the free energy per site  $f_t(T)$  in Eq. (4) when  $t = 0$ , where the TTM coincides with the octahedral model. The triangles and the circles correspond to  $f_t(T)$  calculated under fixed and free boundary condition, respectively.

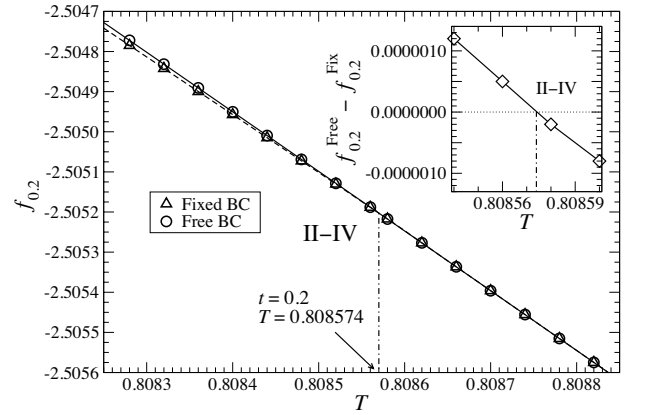


FIG. 8. The free energy per site  $f_{t=0.2}(T)$  around the II-IV phase boundary calculated for both fixed and free boundary conditions; the inset show their difference.

Again we observe the crossover in  $f_t(T)$ , where the lines crosses at  $T_0 = 0.808574$ . The latent heat is estimated as  $Q = 0.028$ . These results support the presence of a weak first-order phase transition along the II-IV phase boundary. It should be noted that our result do not agree with the recent Monte Carlo study, where the second-order phase transition is conjectured for the octahedral model<sup>3</sup>.

Since the TTM coincides with the tetrahedral model in the limit  $t = 1$ , the critical temperature  $T_c$  in this limit can be calculated exactly as  $T_c = 4J/(3 \ln 3) \approx 1.21365 J$ , and the transition belongs to the 4-state Potts universality class. In this case, numerical confirmation is not straight forward, because of the nature of Berezinskii-Kosterlitz-Thouless (BKT) transition<sup>21-23</sup>. Along the III-IV phase boundary, we observed a very slow convergence in free energy with respect to the system size  $L$ , which suggests the presence of BKT transition in the whole part of the III-IV boundary. We leave the confir-

mation of this conjecture for a future study.

#### IV. DISCUSSION AND CONCLUSIONS

We have investigated the phase diagram and the thermodynamic property of the truncated tetrahedral model by means of the CTMRG method. Entanglement entropy is used for the determination of phase boundaries. In the intermediate temperature region, the model shows either  $Z_2$  symmetry or  $D_3$  one, and the phase boundary between these intermediate phases is of the 1<sup>st</sup> order. It is shown that the phase transition from the completely disordered high-temperature phase to the phase II, which has  $Z_2$  symmetry, is of the first order, where the latent heat is very small.

The presence of the weak first order transition in the octahedral model draws an attention to icosahedral and dodecahedral models, which have larger local degrees of freedom than the icosahedral model. To perform CTMRG calculation in a stable manner for these many-state model is a kind of numerical challenge, since the memory requirement is severe at the moment.

#### ACKNOWLEDGMENTS

This work was supported by the projects QIMABOS APVV-0808-12 and VEGA-2/0130/15. T. N. and A. G. acknowledge the support of Grant-in-Aid for Scientific Research. R. K. acknowledges the support of Japan Society for Promotion of Science P12815.

- 
- \* andrej.gendiar@savba.sk
- <sup>1</sup> N.D. Mermin and H. Wagner, Phys. Rev. Lett. **17**, 1133 (1966).
  - <sup>2</sup> F.Y. Wu, Rev. Mod. Phys. **54**, 235 (1982).
  - <sup>3</sup> T. Surungan, The 2nd International Conference on Theoretical Physics Palangkaraya University (2012).
  - <sup>4</sup> T. Surungan, N. Kawashima, and Y. Okabe, Phys. Rev. B **77**, 214401(2008).
  - <sup>5</sup> T. Nishino and K. Okunishi, J. Phys. Soc. Jpn. **65**, 891 (1996).
  - <sup>6</sup> T. Nishino and K. Okunishi, J. Phys. Soc. Jpn. **66**, 3040 (1997).
  - <sup>7</sup> R.J. Baxter, *Exactly Solved Models in Statistical Mechanics* (Academic Press, London, 1982).
  - <sup>8</sup> J. Genzor, V. Bužek and A. Gendiar, Physica A **420**, 200 (2015).
  - <sup>9</sup> H.F. Trotter, J. Math. **8**, 887 (1958).
  - <sup>10</sup> M. Suzuki, J. Phys. Soc. Jpn. **21**, 2274 (1966).
  - <sup>11</sup> M. Suzuki, Prog. Theor. Phys. **56**, 1454 (1976).
  - <sup>12</sup> E. Fradkin and L. Susskind, Phys. Rev. D **17**, 2637 (1978).
  - <sup>13</sup> A. Osterloh, L. Amico, G. Falci, and R. Fazio, Nature **416**, 608 (2002).
  - <sup>14</sup> T.J. Osborne and M.A. Nielsen, Phys. Rev. A **66**, 032110 (2002).
  - <sup>15</sup> G. Vidal, J.I. Latorre, E. Rico, and A. Kitaev, Phys. Rev. Lett. **90** 227902 (2003).
  - <sup>16</sup> F. Franchini, A.R. Its, B-Q. Jin, and V.E. Korepin, J. Phys. A **40** 8467 (2007).
  - <sup>17</sup> E. Ercolessi, S. Evangelisti, F. Ravanini, Phys. Lett. A **374**, 2101 (2010).
  - <sup>18</sup> P. Calabrese and J. Cardy, J. Stat. Mech.: Theor. Exp., P06002 (2004).
  - <sup>19</sup> T.W. Burkhardt and J.M.J. vanLeeuwen, *Real-Space Renormalization*, Topics in Current Physics vol. **30**, (Springer, Berlin, 1982), and references therein.
  - <sup>20</sup> T. Nishino, K. Okunishi, and M. Kikuchi, Phys. Lett. A **213**, 69 (1996).
  - <sup>21</sup> V.L. Berezinskii, Sov. Phys. JETP **32**, 493 (1971).
  - <sup>22</sup> V.L. Berezinskii, Sov. Phys. JETP **34**, 610 (1972).
  - <sup>23</sup> J.M. Kosterlitz and D.J. Thouless, J. Phys. C **6**, 1181 (1973).